Mars Reconnaissance Orbiter Capabilities in Support of Human Mars Missions

Paul D. Fieseler,[*] Mazen M. Shihabi[†], Armin Kleinböhl[‡] and Leslie K. Tamppari[§]
Jet Propulsion Laboratory, California Institute of Technology, Pasadena, California 91109, USA

Shane Byrne, Alfred S. McEwen
Lunar and Planetary Laboratory, The University of Arizona, Tucson, AZ, 85721, USA

Nathaniel E. Putzig[**]
Planetary Science Institute, 405 Urban Street, Suite 300, Lakewood, Colorado 80228, USA

and
Liliya V. Posilova[††], Bruce A. Cantor[‡‡] and Gunnar Speth[§§]
Malin Space Science Systems, San Diego, California 92191, USA

The Mars Reconnaissance Orbiter is uniquely qualified to meet objectives required by human missions to Mars. Landing site characterization capabilities include imaging for boulders and terrain difficult for landing and/or driving, understanding soil compaction for future construction, plus locating resources such as sub-surface ice deposits and caves. During the entry, descent and landing phase, the UHF radio can provide real-time data return, while several instruments can provide weather and atmospheric density information. The high-resolution imager can capture photos of a vehicle mid-descent and after touchdown. These capabilities could prove vital for determining the root cause after an anomaly. Once human presence on Mars is established, the UHF radio can provide positioning information, relay data from equipment placed outside of direct communication with the landing site and possibly serve as a back-up communication system during extravehicular activities. Other

[*] MRO Chief Engineer, 394A Mission System Leadership, AIAA Professional.
[†] Group Supervisor, 337K – Communication Architecture and Operations.
[‡] MRO MCS Principal Investigator, 3222 - Planetary and Exoplanetary Atmospheres
[§] MRO Project Scientist, 3222 - Planetary and Exoplanetary Atmospheres
[**] MRO SHARAD US and Deputy Team Lead, PSI Associate Director, Senior Scientist
[††] Deputy Principal Investigator for CTX, Malin Space Science Systems.
[‡‡] Senior Staff Scientist, Malin Space Science Systems
[§§] Staff Scientist, Malin Space Science Systems.

MRO capabilities include creating stereo maps for extravehicular route planning, dust storm prediction and monitoring, atmospheric density measurements for aerobraking, improvement of spacecraft ephemerides to assist with precisely targeted landings and finding lost hardware in orbit and on the ground.

I. Introduction

The Mars Reconnaissance Orbiter (MRO) spacecraft was launched in 2005, began aerobraking into orbit at Mars in early 2006 and has been in its science orbit since September 2006 [1]. It is in a highly inclined orbit with a periapsis of 250 km near the south pole and an apoapsis of 320 km near the north pole. The orbit is sun-synchronous and maintains a Local Mean Solar Time (LMST) between 2 and 4 pm over the lit side [2]. The spacecraft typically flies with the main instrument deck oriented in the nadir direction as shown in Fig. 1 but often is rolled about its along-track axis to improve radar or UHF signal strength, or to image off-nadir features perpendicular to the ground track direction. MRO possesses twin solar arrays that articulate to provide ~ 2 kW of power. A 3 m diameter high gain antenna downlinks data in X-band to 34-meter stations of NASA's Deep Space Network at rates up to 6 Mb/sec.

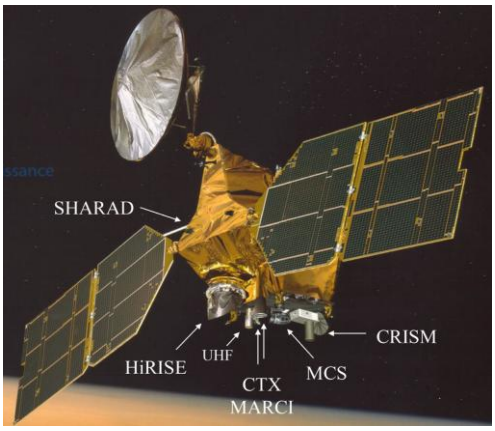

Fig. 1 The Mars Reconnaissance Orbiter

A. Equipment Relevant to Human Mission Support

The spacecraft carries the following equipment relevant to providing future support to a human mission to Mars.

CTX – Context Imager. This instrument is a line scanner that provides 6 m/pixel scale over a 30 km wide swath [3]. CTX has covered essentially 100% of the Martian surface to date and is able to repeat coverage for monitoring surface changes. CTX is now building stereo coverage of Mars using images taken across multiple orbits.

Electra – a UHF radio. The Electra radio carried by MRO is compatible with the Mars Relay network CCSDS proximity-1 link protocol. MRO Electra is frequency-agile; it can operate its forward link (MRO to another vehicle) anywhere within the 435-450 MHz sub-band, and the return link (another vehicle to MRO) anywhere within the 390-405 MHz sub-band [4]. Its adaptive data rate capability allows it to autonomously select the best data rate throughout the pass from all powers of 2 from 1 kbps up to 2,048 kbps using a variety of encoding schemes. Electra can provide radiometric tracking to support in-situ surface positioning, or in-orbit navigation. MRO carries two Electra radios, one of which is a currently never-used spare.

HiRISE – High Resolution Imaging Science Experiment. With its 25–30 cm pixel scale (<1 m resolution), HiRISE remains the best camera at Mars for a variety of purposes related to human exploration [5]. The camera can see a ~ 5 km wide swath in monochrome and a 1.2 km wide, 3 color central stripe. Using multiple orbits with similar lighting conditions, stereo images are produced. HiRISE is a line scanner with Time Delay Integration rather than a framing camera.

MARCI – Mars Color Imager is a wide-field pair of cameras that provide daily global coverage of weather, ozone (a water vapor proxy) and atmospheric dust [6]. The instrument provides an image scale between 1 and 30 km across two ultraviolet and five visible bands.

MCS – Mars Climate Sounder. MCS is a thermal infrared radiometer covering nine wavelength bands between 0.3 and 45 μm [7]. It measures radiance profiles when pointed at the Mars limb, from which vertical profiles of temperature, dust extinction and water ice extinction are operationally retrieved between the near-surface and 80-90 km altitude with a vertical resolution of ~5 km [8]. In addition, dust and water ice column optical depths as well as surface brightness temperatures are derived [9].

ONC – Optical Navigation Camera. This camera couples a 1024x1024 pixel CCD, a 450-600 nm filter with optics that provide a 500 mm focal length and a 1.4 degree square field of view. ONC is optimized for detecting dim objects against the dark background of space [10]. Originally intended to use Phobos and Deimos for a navigation demonstration, the camera has also been used to search for moonlets of Mars and a derelict spacecraft in Mars' orbit.

SHARAD – Shallow Radar sounder. SHARAD provides ionospheric, surface and sub-surface sounding with a vertical resolution of ~15 m to depths of 2 km [11]. It can detect water ice in support of human missions [12]. Recent advancements in operations have allowed SHARAD to improve its gain by an order of magnitude by conducting very large rolls of the spacecraft [13].

CRISM – Compact Reconnaissance Imaging Spectrometer for Mars. CRISM's primary role has been mineral detection [14]. It lost capability to utilize infrared channels when its suite of cryocoolers failed but it retains some capability using its remaining visible channels. While the instrument remains functional, it was turned off in 2022 due to budget reductions. Its capabilities are not further considered in this paper.

B. Spacecraft Health

Overall, the spacecraft is in excellent health. Three significant components have exceeded their qualification limits, 1) the primary X-band Travelling Wave Tube Amplifier (TWTA) life, 2) the number of revolutions of one high gain antenna gimbal and 3) the life of the Ultra Stable Oscillators (USOs). The TWTA shows current and voltage degradation consistent with only being at the mid-point of its life. The high gain gimbal shows no unusual friction or other unexpected behavior, and the mission could continue without it at the cost of rolling the spacecraft body to compensate for the lost degree of freedom. The USO provides the sole, but cross-strapped, clock source for the Electra radio. The primary USO was turned off in 2018 after exhibiting unexpectedly large phase noise. The secondary unit remains healthy.

All other consumables including heater and power switch cycles, thruster valve usage, and reaction wheel revolutions are under qualification limits. MRO always maintains a solar array power margin of > 1 kW. MRO's batteries retain ~2x the capacity required for the longest duration eclipse.

One of the two Inertial Measurement Units (IMUs) has begun an aging associated decline. The other IMU remains nominal, and the projection is that the pair will serve until late 2038 without any operational modifications that could further extend life.

Propellant is the nearest term mission-ending consumable that MRO has. At the current hydrazine usage rate of ~ 10 kg/year, we expect MRO to survive until early 2038. Currently unimplemented conservation efforts could extend this date farther into the future.

1. *HiRISE Health*

After approximately 20 years in space, the HiRISE camera continues to return the highest resolution orbital images of Mars by currently working around two limitations. A brief summary follows here; see [15] for additional details.

Starting soon after launch, data from some of the 14 detectors began showing a form of electronic noise that was attributed to bit flips when the analog CCD signal was digitized. The HiRISE Analog-to-Digital Converters (ADCs) digitize CCD outputs as 14-bit numbers so flipping minor bits results in minor noise; however, flipping major bits causes major errors in those pixel values (including negative numbers later encoded as zeros). Bit flips have increased in their severity over the length of the mission and are now present to some extent in almost all detectors. This noise can be suppressed by increasing instrument electronics temperatures; however, starting an image at higher temperature limits its maximum length. Throughout the mission, HiRISE has increased temperatures at the start of imaging and raised maximum temperature limits to balance the needs to lower bit flips, to have reasonable image lengths, and to avoid the highest temperatures that might damage parts. Additional strategies like changing the ADC settings have also produced improvements. Full resolution images are more susceptible to bit flips than binned images (and some ADCs are worse than others). As bit flips worsen, HiRISE has taken more bin-2 data (still the highest resolution orbital imagery at Mars) and uses shorter bin-1 images over sites where the image rationale requires it (e.g. landing site verification). In future years, HiRISE will balance more bin-2 imaging with additional risk from further raising instrument temperatures.

Since launch in 2005, two of the fourteen HiRISE detector readout modules have failed. One of the RED modules at the edge of the field of view (FOV) failed in 2011, reducing the FOV by 10%. In 2023, another red module (RED4) in the center of the FOV began failing. Commanding of this detector was suspended in 2024. An effort to resume use in early 2025 yielded temporary success, but increasing failures and meant this effort was again suspended. In mid-2025, commanding has resumed with a success rate of ~40%. The image gaps from the RED4 failure are being filled by the IR-filter data. Although lower SNR than RED, the IR filter fills these gaps seamlessly in most cases and can also be used in DTM production from stereo pairs.

2. *MCS Health*

After nearly 20 years of operations, the elevation actuator of MCS used for conducting surface and calibration views has become unreliable. Currently MCS views the atmosphere at a fixed elevation angle in limb geometry in a direction perpendicular to the MRO orbit track, similar to cross-track limb observations that were carried out periodically throughout the mission. Views of space for calibration as well as surface observations are now conducted by rolling the MRO spacecraft in lieu of actuator movement.

3. Other Instrument Health

The other science instruments, CTX, MARCI and SHARAD, are all operating at full capacity. The Electra is nominal except for rare (~1 per year) resets. A redundant Electra unit has never been powered in flight.

II. Capabilities for Landing Site Selection

A. Characterization of Landing Site Safety

1. HiRISE Terrain Observations

HiRISE images and derived stereo products have revolutionized the safety validation of Martian landing sites. HiRISE data at 25cm/pixel (and DTMs at 1m/pixel) has guided the landing site selection for Phoenix [16-17], Mars Science Laboratory [18], InSight [19] and the Perseverance rover [20], as well as the planned Rosalind Franklin Rover [21].

Boulder counts derived from HiRISE data yield direct information about lander-scale hazards. HiRISE data allows the size-frequency distribution of boulders to be constrained down to the 1-meter scale. Comparison with post-landing surface data at the landing sites of Viking 2 and Insight show extrapolation of these counts to even smaller sizes remains valid [22]. Early HiRISE images showing surface boulders (Fig. 2) led to a revision of the Phoenix landing site for safety reasons [16-17]. HiRISE DTMs are typically gridded at post spacings of one meter and can yield slopes down to that scale [23]. Direct measurement of surface roughness from these DTMs aid in landing site characterization. Both HiRISE images and DTMs can characterize larger hazards such as impact craters and aeolian ridges.

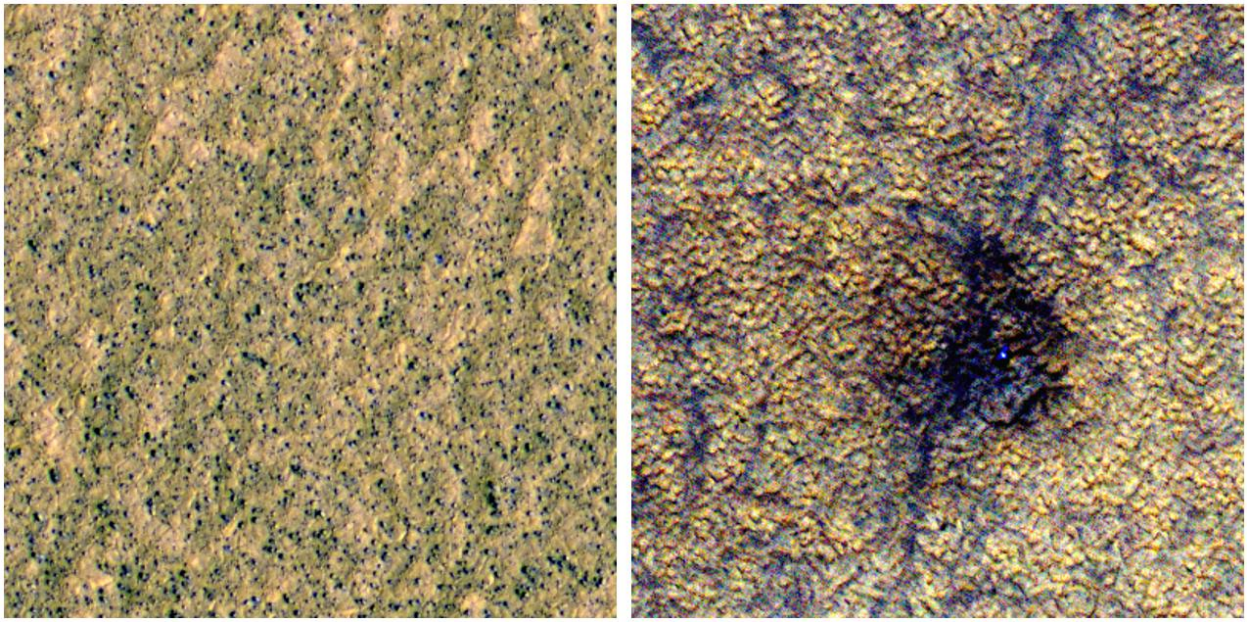

Fig. 2 HiRISE views showing (left) a candidate Phoenix landing site that was abandoned due to high boulder counts (TRA_000881_2475, 100 m across) and (right) the final Phoenix landing site in a boulder-free area (PSP_008644_2485, 100 m across). The bright blue spot is the Phoenix lander.

Future candidate human landing sites have been identified in several workshops. HiRISE has imaged several dozens of these sites, but many more remain. Characterizing a single site for robotic landings often requires dozens of images including stereo coverage. Human missions may have smaller landing ellipses, but clearly much more data will be required at HiRISE scales. Outside of these sites, the HiRISE dataset has covered an area equivalent to 5% of the planet; however, many of these images overlap to investigate changes or provide stereo coverage, so unique coverage is lower.

2. MCS Measurements of Local Surface Properties, Temperature Extremes

Thermal inertia derived from MCS measurements constrains the porosity and degree of cementation of the soil at a potential landing site, hence providing information on its stability for landed vehicles and suitability for subsequent building construction. In addition, MCS measurements provide information about the thickness and properties of the overburden over a potential ice layer. Furthermore, MCS surface temperature, together with dust optical depths, can

be used to estimate surface temperature extrema expected at a landing site, which is critical for landed vehicle thermal design.

3. SHARAD and CTX Measure Surface Roughness

SHARAD reflections from the surface can be used to assess roughness of the terrain at ~15-m scales that are intermediate to that provided by HiRISE and MOLA [19,24-26]. Especially where HiRISE coverage may be incomplete, this additional source of information may be important to evaluating landing site safety and trafficability. CTX also offer intermediate-scale measurements of surface roughness via stereo terrain mapping.

B. Landing Site In-situ Resource Identification

1. Multi-instrument Assessment of Water Ice Resources

No instrument on MRO or any other Mars spacecraft has been designed expressly for identification of in situ resources. However, many instruments designed for other scientific purposes have collected data that may be used for that purpose. During the 2015 First Landing Site/Exploration Zone Workshop for Human Missions to the Surface of Mars, a consensus was reached that water is the most critical of in situ resources, with buried ice in the mid-latitudes being a primary source of such water [27]. It was also realized at that time that no concerted effort had yet been made to examine all available datasets that inform the presence and nature of buried ice on Mars. Therefore, NASA initiated a call in 2017 for pilot studies to assess buried ice across an area in Arcadia Planitia that had shown indications of buried ice concentrations in excess of pore space [28] Two complementary studies were selected, which were later merged and expanded across the northern hemisphere into a single effort known as the Mars Subsurface Water Ice Mapping (SWIM) project [29]. The SWIM Project has been combining data on near-surface hydrogen (from the Odyssey Gamma Ray Spectrometer instrument), surface temperatures (from the Mars Global Surveyor Thermal Emission Spectrometer instrument and MCS), radar surface and subsurface reflectivity from SHARAD, and geomorphology (from CTX and HiRISE images and MGS Mars Orbiter Laser Altimeter topography) to infer where ice is most likely to be present in the Martian midlatitudes. The southern hemisphere was added in a later stage of the project [30]. In the latest stage of work, the geomorphic mapping was refined and the integrated ice consistency from the various datasets was used to establish ice exploration zones that are intended to inform future efforts to better

establish the depth to ice, which is not well constrained by current instruments, in areas of interest for future human landing sites [31] Radar SAR imaging and higher frequency sounding are primary means being examined for this purpose [32].

2. *Direct Detection of Impact-exposed Water Ice by CTX and HiRISE*

CTX is a key instrument in the discovery of fresh impact craters on Mars, with new impacts detected on a near-weekly basis. Some reveal bright material interpreted as exposed subsurface ice – critical for understanding near-surface volatile distribution and assessing potential water resources for future human exploration. Fig. 3 shows one such icy crater at ~44°N, captured in CTX image B19_016954_2245_XI_44N195W, where bright material was later confirmed as exposed ice in a follow-up HiRISE observation. The most equatorward new icy impact crater discovered by CTX to date is located at 35°N. We are actively working to detect additional icy impacts and to determine how close to the equator ice can be exposed; CTX's broad coverage and monitoring cadence make it a critical tool in this effort.

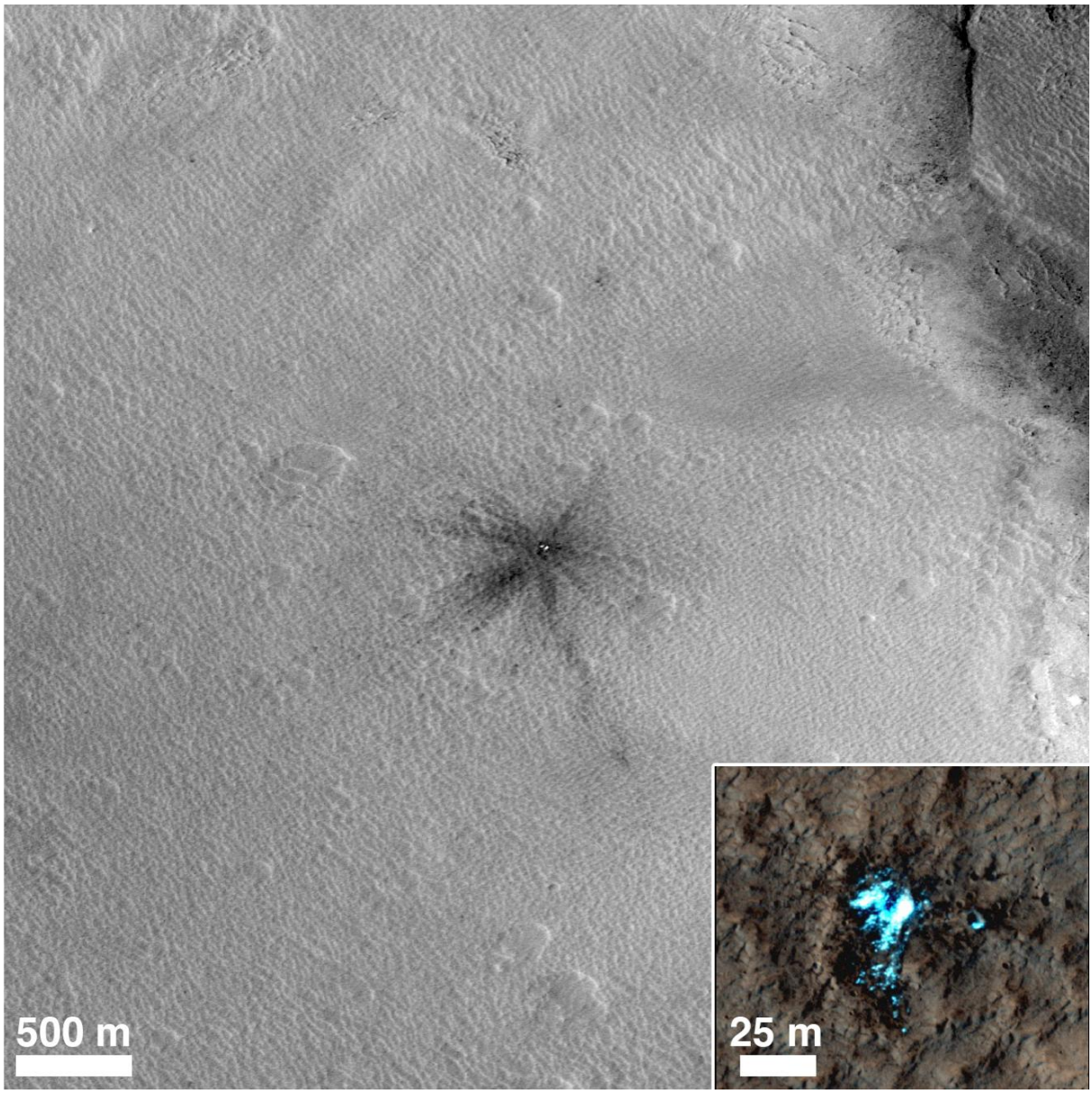

Fig. 3 New impact crater at ~44.2°N, 164.2°E, captured in CTX image B19_016954_2245_XI_44N195W. Bright material in and around the crater is interpreted as exposed subsurface ice. The crater was first identified in January 2010 CTX image; it was absent in earlier coverage from July 2008. Inset: HiRISE image ESP_016954_2245 shows a higher-resolution view. North is up; illumination is from the upper left. NASA/JPL-Caltech/MSSS/University of Arizona

4. Thermal Detection of Water Ice by MCS

MCS can support the characterization of in-situ resources by deriving the depth of a water ice table in the subsurface (see also section B1, above). Subsurface water ice influences the seasonal trend of the surface temperature.

The measured surface temperature trend by MCS can be modeled with a two-layer thermophysical model assuming water ice as the lower material [33] The approach is sensitive to water ice within about 1 m of the surface. It can be applied poleward of roughly 30° latitude and yields results with about 6-7 km spatial resolution.

5. HiRISE and CTX Ancillary Resource Detection

Both imagers can support the discovery of caves [34] and identify accessible geologic materials that may be useful for construction.

C. Landing Site Terrain Relative Navigation

Precision landing systems that rely on high-resolution terrain maps—like those generated for Terrain-Relative Navigation (TRN) during the successful landing of the Mars 2020 rover—will be essential for future human landings on Mars. CTX and HiRISE have demonstrated the ability to meet stringent operational demands by supporting TRN, acquiring stereo images under mission-defined constraints on lighting, dust, and timing. For the proposed future Mars Sample Return mission, even tighter requirements were specified, including the generation of flight-quality appearance and elevation maps. These maps will be used to support precision localization during descent, with a targeted landing accuracy of <60 meters. CTX acquired the necessary stereo pairs under strict conditions—meeting detailed requirements on sun angle, dust content, convergence angle, and timing between stereo acquisitions.

Human landing missions will require even greater precision. To support this, enhanced landing systems depend on high-quality stereo maps generated from images acquired under lighting conditions that match the expected landing season and time of day. The CTX camera's 30-km wide swath at 6 m pixel scale enables the creation of these maps in a timely manner. The HiRISE 25 cm pixel scale captures fine detail improving the TRN utility. The combined ability to deliver reliable, high-resolution mapping under mission-driven constraints makes MRO a vital contributor to future surface exploration success.

III. Capabilities for Entry, Descent and Landing Support

MRO has supported the entry, descent and landing (EDL) phases for Mars Phoenix, Mars Science Laboratory, Insight and Perseverance missions, through the use of RF communication, atmospheric measurements, and visual tracking.

A. Electra UHF Support During EDL

A driving reason for providing direct UHF support during EDL is to provide data in the event of a major anomaly, as there is no current capability to retrieve a "black box". A secondary reason is to allow ground controllers to respond to any critical anomalies post-landing. Public engagement with the landing is also a consideration.

Communication from the lander directly to the Earth is difficult during EDL since the many constraints on landing time and location may mean that the Earth is not in view for part of or all the descent. MRO availability can often be assured, since MRO typically phases along its orbit to overfly the descending vehicle and, to some extent, MRO can also adjust the plane of its orbit to minimize range. When the Earth is in view, a high gain or medium gain antenna is needed to close the link with even a large ground station like Greenbank, but protruding antennas are incompatible with the aerodynamic requirements of a descending vehicle. Even a patch array antenna placed on the aeroshell exterior will have difficulty maintaining earth-point given the dynamics of the vehicle in descent. A hypothetical optical comm link would have the same difficulty, plus the risk of attenuation by clouds, dust and CO2 absorption in the case of an infrared signal.

Starting with the 2008 Phoenix lander mission, MRO was assigned the task of providing the Entry, Descent and Landing support by performing an open-loop recording of the transmitted UHF waveform of the descending vehicle. In the Open-loop recording mode, MRO Electra can acquire a high-fidelity recording of a UHF signal, over a Nyquist-sampled bandwidth at rates up to 150 kHz, enabling ground post-processing to reconstruct the observed spectrum as well as to demodulate a high-rate telemetry signal [4]. For the Phoenix mission, the data rate during EDL was 32 kbps. MRO Electra also supported the MSL rover mission (2012) as well as the InSight lander mission (2018) during EDL using the Open-Loop Recording (OLR) mode. The data rate during both mission EDL events was 8 kbps.

For the Perseverance mission, MRO was asked to develop a “bent-pipe” function [35]. The bent-pipe capability is the ability to capture the lander’s telemetry onboard an orbiter which then relays it to the Earth with a < 10 second delay. See Fig. 4 for more details. Electra software, MRO spacecraft flight software and DSN software were updated to provide this capability, and all remain in place as a standard MRO service.

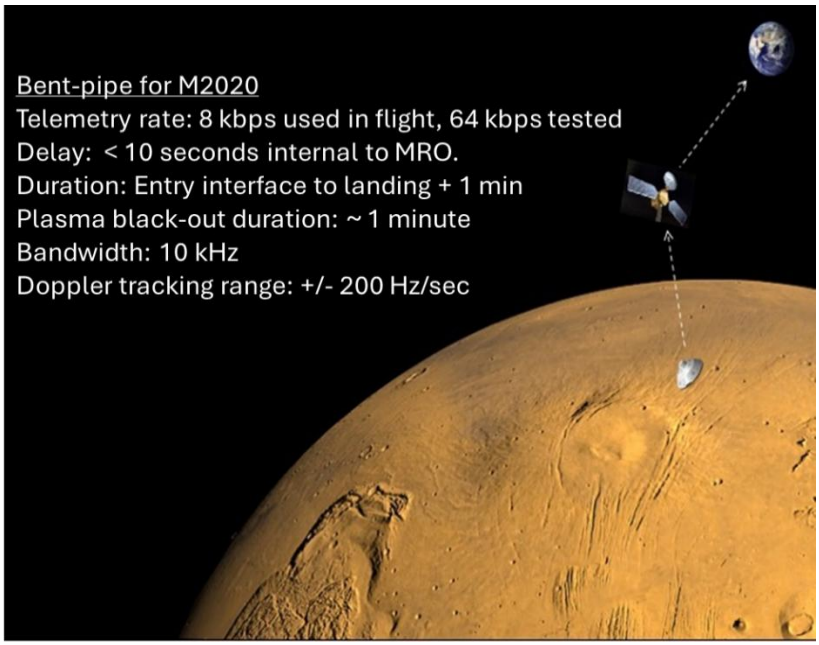

Fig. 4 MRO Bent-Pipe Relay Support Concept

B. MCS Weather and Atmospheric Data Collection

MCS supported the EDL activities of Phoenix in 2008 [36,37], MSL in 2012 [38,39], InSight in 2018 [40,41], and Mars 2020 in 2021. EDL activities typically consist of several phases, all of which are supported by MCS. In a first phase, the selection of a landing site is supported by evaluating the “flyability” of the atmosphere over candidate landing sites [42]. In a second phase, specific atmospheric risks to landing are characterized with respect to expected

perturbations in atmospheric density, as well as wind speed and wind shear. A “Council of Atmospheres (CoA)” evaluates atmospheric temperature and density structure as well as wind for various dust scenarios using mesoscale modeling [42]. MCS provides input to models and supports the validation of modeling activities with atmospheric temperature and dust information. The third phase consists of real-time support and covers the period from a few weeks prior to EDL through EDL [42]. MCS provides profiles of temperature, dust, and water-ice opacity as a function of pressure and altitude near the landing site, initially weekly or every two weeks. In the last week prior to EDL this information is provided daily as part of MRO’s critical event coverage, with a focus on detecting the potential development of major dust storms and their effect on atmospheric temperature and density structure. The measurements are compared with modeled profiles to evaluate whether the dust scenario assumed in the model is still realistic or should be modified. We envision that EDL in support of human missions will involve similar atmospheric characterizations and MCS would be able to contribute to them in the same way as it has contributed to the EDL of robotic missions.

In addition to observations leading up to EDL, MCS observed the atmosphere post-landing, typically one MRO orbit (~2 hours) after touchdown. Fig. 5 shows a comparison of the predicted atmospheric temperature profile for Phoenix EDL and the measured profile by MCS after EDL in comparison to the reconstructed temperature profile from the Phoenix trajectory. The overall agreement between the MCS measurement and the reconstructed profile is excellent, slight differences at higher altitudes might be related differences in local time and associated changes of the atmospheric structure due to atmospheric tides. MCS would provide such observations also for future human missions as well as precursors to human missions, e.g., conducted to demonstrate landing of heavy payloads on Mars. MCS profiles would serve as a comparison to reconstructed entry profiles or, in case of an anomaly during EDL, provide information about the atmospheric structure leading up to the anomaly.

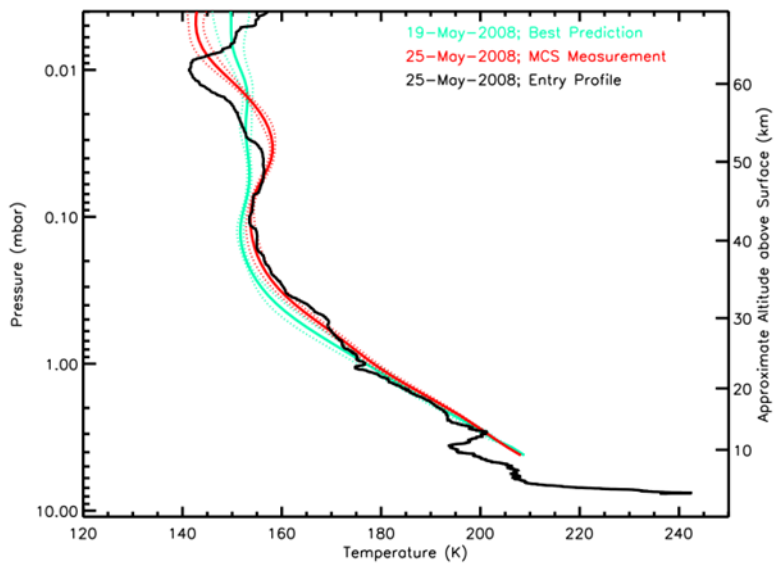

Fig. 5 Predicted atmospheric temperature profile for Phoenix EDL (green), measured atmospheric temperature profile by MCS above the Phoenix landing site shortly after EDL (red), and temperature profile reconstructed from the Phoenix entry trajectory (black).

C. MARCI Weather and Atmospheric data collection for EDL, Aerobraking.

MARCI imaging over the course of a Martian sol, 12-plus orbits, provides a daily global view of the dayside of the planet in seven color channels, five visible (437, 546, 604, 653, and 718 nm) and two UV (258, and 320 nm). The surface sampling scale in the visible bands is 1 km at the nadir, 3.75 km at the cross-track limb, and for the UV, 8 km at nadir and 30 km at the cross-track limb. These channels have been used to track surface albedo changes [43] polar cap recessions [44,45], ozone [46] and synoptic meteorological phenomena, including condensate (water-ice and CO_2) clouds [43,47-49], and dust lifting events from large dust devils to local dust storms to planet-encircling dust events [44,50]. The daily monitoring and tracking of dust storms across the planet can be important because storms can change the local and regional thermal structure of the atmosphere which can impact aerobraking and EDL accuracy. This monitoring has been used to support landing site selection for the MSL, Mars2020 [50], and ESA's planned Rosalind Franklin rover, as well as support for EDL of NASA rover and lander missions. The MARCI weather monitoring has also been used to support mission planning and operations for the Phoenix Lander and MER rovers, as well as orbital insertion for MAVEN and aerobraking and orbital correction maneuvers for MRO and MAVEN. Daily-to-biweekly weather reporting in the form of weather updates (Fig. 6) and forecasts of storm activity has been

provided to all NASA surface and orbital missions since 2006. Now into an eleventh Mars year of monitoring, MARCI's global eye in the sky capability continues to provide uninterrupted support of all NASA assets at Mars.

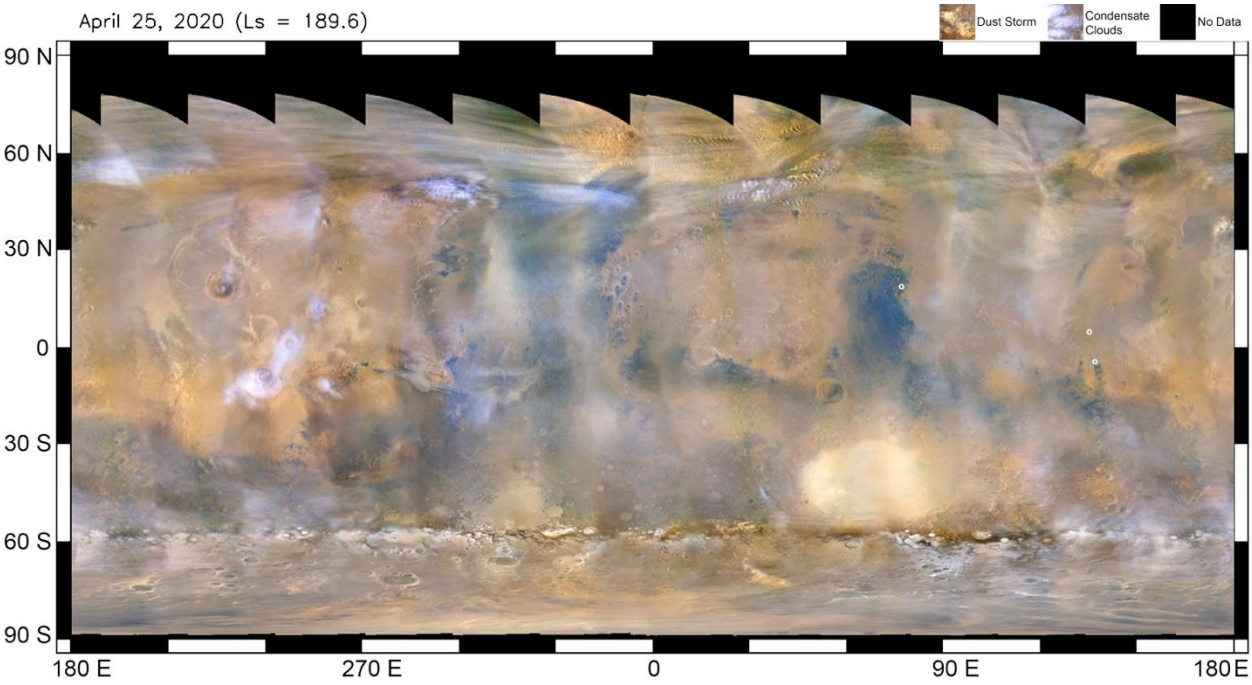

Fig. 6 Synoptic meteorological events, condensate clouds and dust storms as observed in a false color MARCI visible (RGB filters) daily global imaging taken on April 25, 2020. The white circles on the right denote location of the Curiosity and Perseverance Rovers and the InSight Lander sites.

D. Landing Assessment and Reconstruction

1. CTX Monitoring of Descent Vehicle Hardware

CTX has a strong track record of supporting safe landings and site monitoring. It has located and monitored hardware from multiple landed missions, including Phoenix, MSL Curiosity, InSight, and M2020 Perseverance. The primary components (lander, parachute, backshell, and heat shield) were captured within a single CTX image, highlighting the camera's broad coverage and targeting precision [Fig. 7]. In addition, CTX was able to identify more subtle features such as the impact marks from cruise and entry ballast masses from both the MSL and Mars 2020 missions. In fact, CTX captured the Mars Science Laboratory's ballast impact "splotches" within minutes of data return—a testament to the team's experience, agility, and operational readiness. These observations have enabled

engineering teams to compare predicted and actual hardware dispersal patterns, validate hazard maps, and assess surface interactions of entry, descent, and landing systems. Continued monitoring also contributes to estimating resurfacing rates, offering insight into how long surface features—including future human infrastructure—remain detectable on Mars.

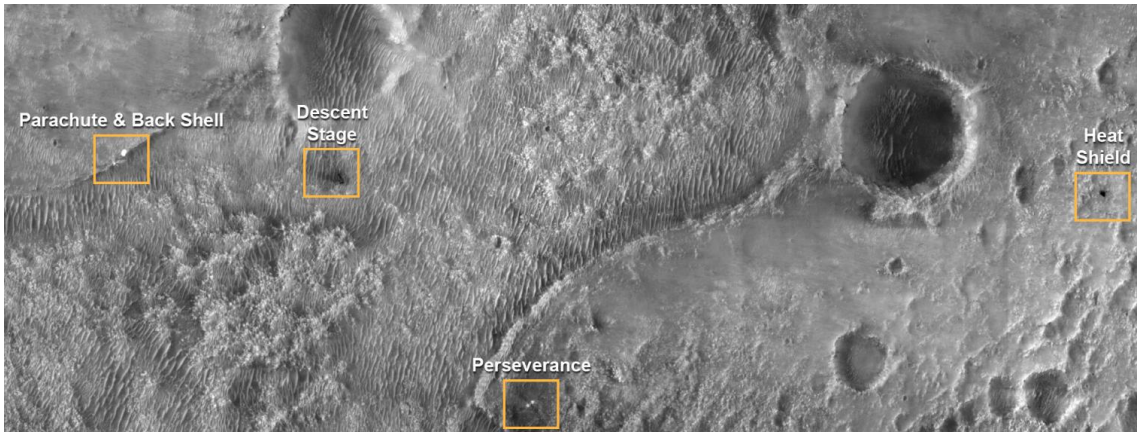

Fig. 7 Photojournal image PIA24333: Perseverance and Mars 2020 Spacecraft Components on the Surface, NASA/JPL-Caltech/MSSS/University of Arizona

2. HiRISE Monitoring of Descent Vehicle Hardware

To support future human missions, orbital high-resolution imagers can help resolve what happened in off-nominal landings and locate the landing sites of hardware that is incapable of broadcasting its own location. HiRISE has supported robotic landings through imaging the landing spacecraft during descent as well as locating landers and associated hardware immediately post landing.

HiRISE descent images of landers on parachutes, Fig. 8, have succeeded for Phoenix, Curiosity, and Perseverance. Such images take months to prepare as MRO is gradually transitioned into an orbit that puts it in the right place at the right time. MRO sweeps the HiRISE FOV across the area of the atmosphere expected to contain the descending spacecraft (typically while it is on its parachute stage). Simultaneous relay of lander data to Earth takes priority so the HiRISE image may be optimal (e.g. Curiosity) or taken when further away (e.g. Perseverance).

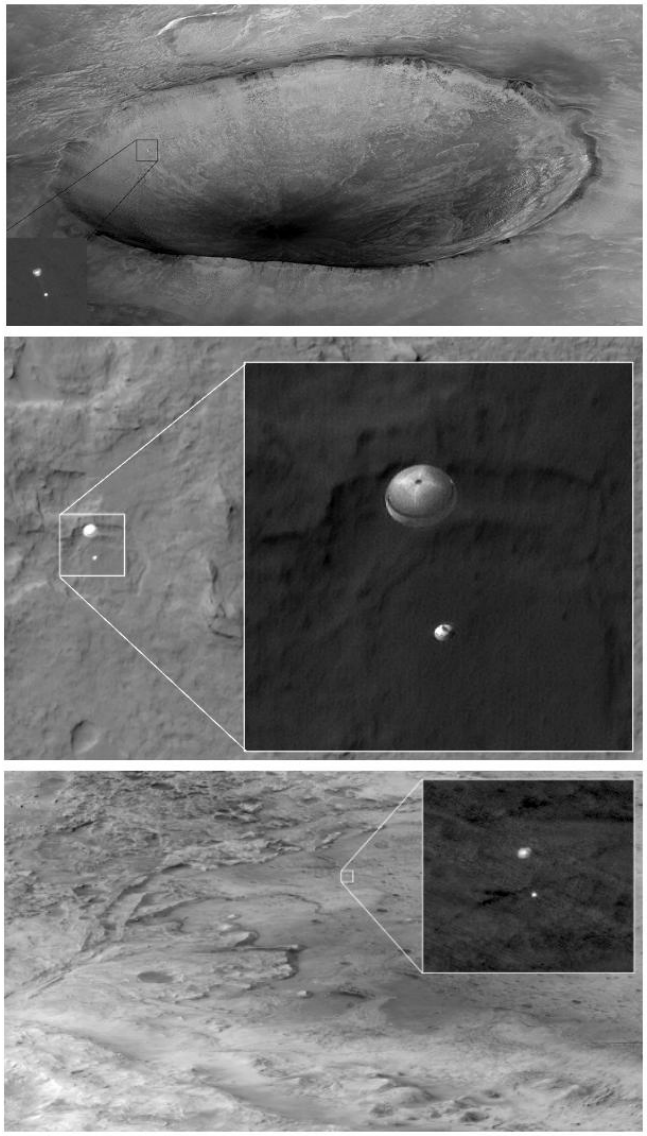

Fig. 8 HiRISE images of spacecraft descending to the Martian surface. From top to bottom: Phoenix (2008); Curiosity (2012); and Perseverance (2021).

Locating the main lander is usually accomplished with its direct-to-Earth transmissions; however, HiRISE data can be used to locate failed landings (Beagle 2, Schiaparelli), inactive landers (Mars 3, Vikings, Pathfinder), and inert hardware (parachutes, heatshields, sky cranes). In some cases, orbital imagery can play a key role in understanding landing failures. Beagle 2 attempted a landing in Isidis Planitia in 2003 and never established contact with the Earth. Higher than anticipated atmospheric dust was implicated as the most likely cause of failure. However, surface glints at the limit of HiRISE resolution were discovered in 2015 and match the expected size and shape of partly deployed

Beagle 2 solar panels [51]. A possible explanation is now that Beagle 2 landed successfully, deployed all but one or two solar panels, and this configuration prevented communication with the Earth. Thus, orbital imaging completely revised Beagle 2's story. Likewise, a set of features consistent with hardware from the Soviet Mars 3 mission has been identified in Terra Sirenum. Mars 3 operated on the surface for only 14 seconds in 1971 and so its position was only approximately known before HiRISE. Data from HiRISE can identify the hardware associated with landing such as jettisoned heat shields and parachutes. The distribution of these hardware elements provide extra information about the landing process and their fading over time constrains the dust fallout rate (Fig. 9).

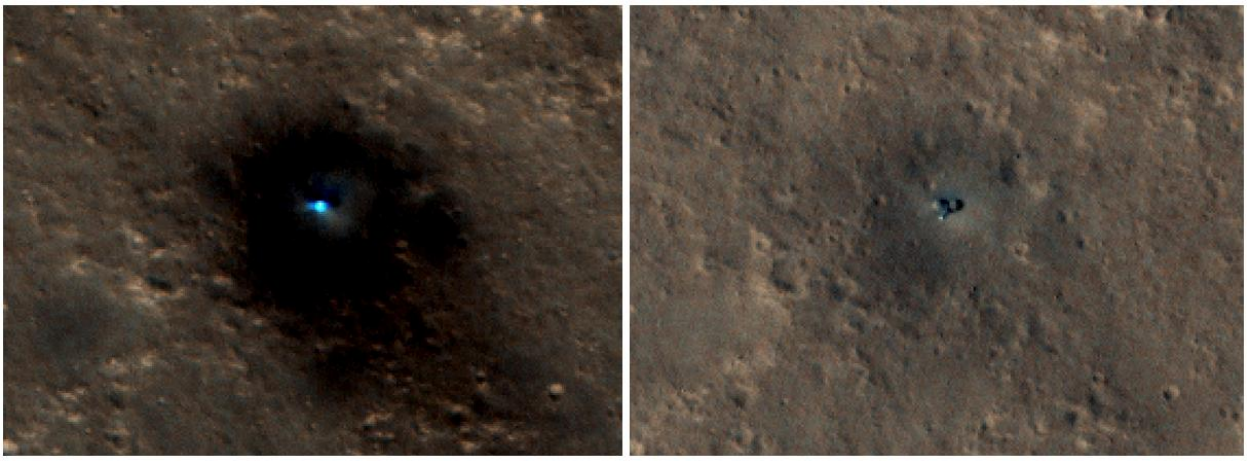

Fig. 9 Accumulation of dust on the Insight lander (shown here in HiRISE images ESP_057939_1845 to ESP_073211_1845) eventually ended its mission by cutting off solar power production.

IV. Capabilities for Landed Operations

A. Electra UHF telecommunications, voice and data support

MRO initiated its relay operations with the Mars Exploration Rovers in 2007. MRO operates in a low-altitude, sun-synchronous orbit with inclination of 93 degrees; and has an orbiting period of almost 2 hours. In general, MRO's high inclination orbit allows for relay access to any point on Mars. Locations near the poles will experience frequent coverage with minimal gaps, while locations near the equator experience less frequent coverage with greater gaps. Due to its slightly elliptical orbit, surface-to-MRO overflight pass duration varies with latitude. Over northern latitudes, MRO is near apoapsis and pass durations are longer. Figure 10 shows the maximum and average values for

pass durations as a function of landed latitude for a 10-deg minimum elevation angle from the surface. Figure 11 shows the number of geometric contact opportunities between MRO and a surface asset at given latitude.

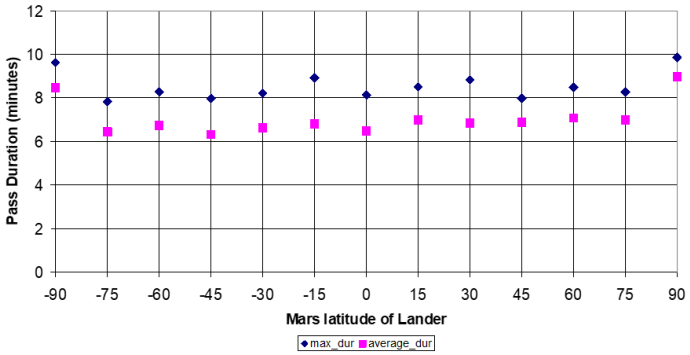

Fig. 10 Pass durations versus latitude for MRO's nominal science orbit with 10 degree elevation mask.

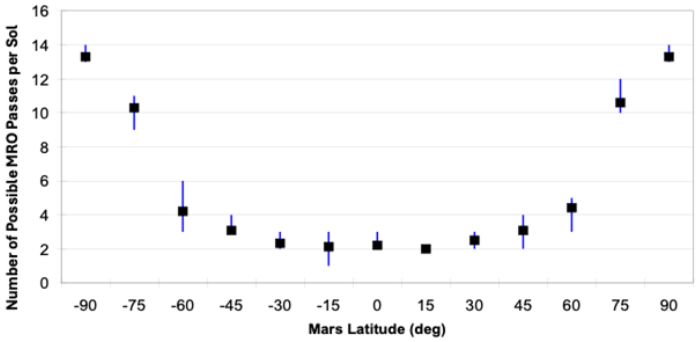

Fig. 11 Number of possible passes with MRO per sol versus surface latitude with 10 degree elevation mask.

MRO Electra firmware and software could be updated to support voice communications. Given that voice communications can be packetized by Pulse Code Modulation (PCM), using the G.711 codec algorithm, resulting in data rate of 64 kbps (8,000 samples/second × 8 bits/sample = 64000 bits/second) [52], this data rate can be easily supported by MRO Electra to provide a backup voice relay communication. The one-way light time delay between the surface and the MRO orbiter, for the longest slant range possible, is on the order of 4 msec allowing the participants to engage in both message-oriented conversation as well as dialog-oriented conversation. Because of the intermittent coverage, the Electra could only be used as a back-up to a higher bandwidth communication system for a human mission. As with EDL support, MRO's orbit can be phased to support high-value, time-limited sessions.

MRO is well suited to support occasional contact with hardware placed beyond the line-of-sight of a human base. Data lost in transmission will be automatically retransmitted with the existing protocols. Remote equipment can store data until MRO passes overhead and initiates the link, in the same fashion that rovers and landers are supported today.

Starting with the surface operations of MSL, Electra has supported frequency-agile operations, data rates up to 2.048 Mbps, suppressed carrier modulation, and a new Adaptive Data Rate algorithm in which the return link data rate is optimally varied throughout the relay pass based on the actual observed link channel characteristics [53]. MRO has supported more than 9,500 relay passes and has relayed more than 2 Tbits of science data from Mars surface since its deployment. MRO supports an average of 2 relay passes per sol per lander and delivers 4.5 Gb of data volume per week.

B. Electra UHF telecommunications, timing and radiometric service

In addition to relay communication services, MRO Electra provides timing and radiometric services (positioning information for vehicles on the surface or in orbit). MRO can provide these services more accurately than any existing Mars orbiter due to its Ultra Stable Oscillator (USO) clock reference. The Timing Data consists of Proximity-1 transfer frame sequence number and Electra time stamps recorded for transmitted and received frames for a Proximity-1 time tagging activity. Timing data, and its associated processing, provide the timing service. When using the timing service, both forward link communications data out of the Electra payload and return link communications data into the Electra payload are tagged with +/-60 ns accuracy relative to the Electra clock. The Radiometric Data measures Doppler shifts, phase, and amplitude of transmitted and received radio frequency waveforms. Like the timing services, the radiometric time tagging, both one-way and two-way UHF radio metric data are time tagged by the Electra Payload with +/-60 ns accuracy relative to the USO clock. In addition to the excellent frequency stability provided by the USO, MRO's near-circular orbit geometry is more conducive to accurate positioning – a frequency source in an elliptical orbit produces a more complex Doppler profile. Because of these factors, the MRO results are more accurate than other extant orbiters (50m, 3sigma for MRO, vs 100m, 3sigma for MAVEN).

C. HiRISE EVA Planning and Search Capability

High resolution imaging can be used to plan surface traverses, identify the current locations of surface vehicles (Fig. 12), and reconstruct the routes taken by them (Fig. 13). HiRISE has demonstrated these capabilities by following the locations of rovers such as Spirit, Opportunity, Curiosity, Zhurong, and Perseverance. In 2005, Opportunity spent several weeks trapped in the 'Purgatory' sand ripple. Subsequent traverse planning utilized HiRISE data to avoid such features and to define most efficient routes to exposures of hydrated sulfate sedimentary rocks [54]. In cases where rover positions were not independently known or are non-cooperative (e.g. Zhurong), HiRISE data can locate these surface assets and see their past routes through the wheel tracks they leave (Fig. 14).

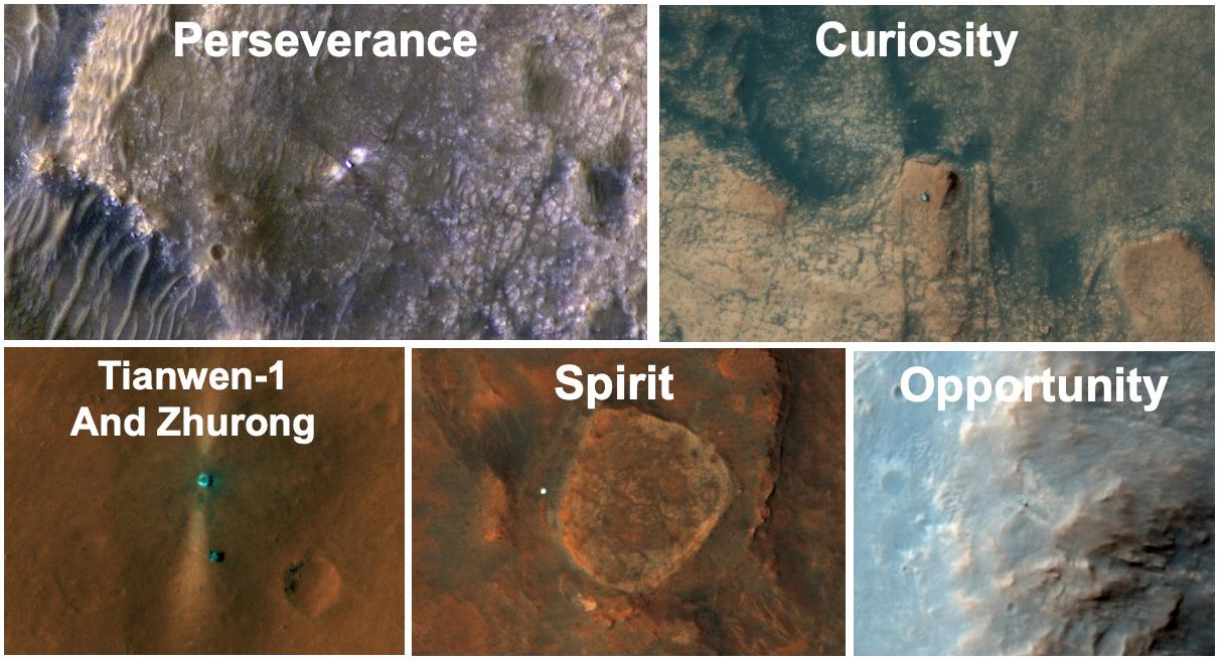

Fig. 12 Various HiRISE views showing the location of mobile rovers on Mars.

Human transports are likely to be larger than the current robotic examples, thus HiRISE-capabilities provide an important backup in off nominal situations where surface assets need to be tracker or located.

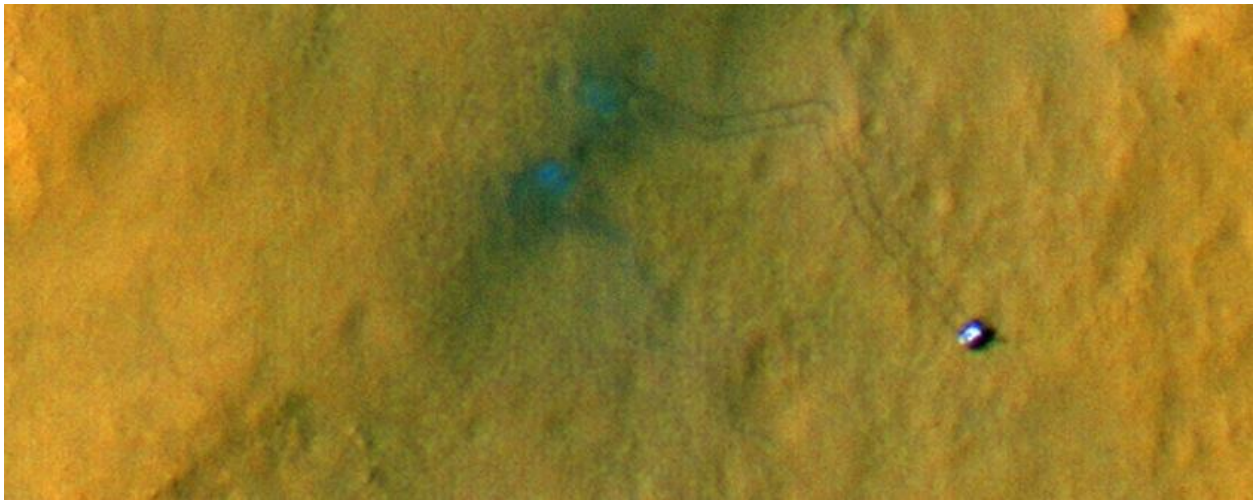

Fig. 13 Curiosity Rover on the move in HiRISE image ESP_028612_1755.

Fig. 14 HiRISE images showing the progress of the Zhurong Rover on Mars. Left panel shows the full route as traced by their wheel tracks, the two panels to the right show no further motion of the rover after 9/8/2022.

D. MARCI and MCS Operational Weather Monitoring

MCS and MARCI would provide operational weather monitoring capabilities to a human landed mission on Mars. During a landed mission, daily weather monitoring would occur similarly to the activities conducted during the week prior to EDL (see sections III B, C). This would allow the detection and characterization of the development of dust storms on a global scale. Such reporting has supported surface operations and science planning of solar and RTG power rover missions, as well as, supporting power management of solar power rovers and landers. Advanced knowledge of dust storm will affect EVA planning and electrical power usage: solar power production will decline due to dust build up on arrays and atmospheric obscuration; nuclear power output may decline if radiators are covered in dust.

V. Ancillary Support

A. Optical Navigation Camera for Tracking Objects in Orbit

MRO's Optical Navigation Camera (ONC) was originally intended as a technology demonstration [55] using optical detection of Mars's moons for enhanced navigation near Mars. The camera was subsequently used in a search for additional tiny moons of Mars; it found none. Recent Mars Sample Return studies have led to work on optically detecting a radio-quiet ascent vehicle or Orbiting Sample [56,57] in low Mars orbit. MRO's 250 km x 320 km orbit allows significant opportunity to image another object in orbit while it appears well above the bright Martian surface and atmosphere. In 2023, MRO successfully carried out successful optical detections of the Trace Gas Orbiter (TGO) spacecraft (a proxy for the Mars Sample Return mission's proposed Orbiting Sample container) at elevations between 2.8 and 13 degrees above the lit Martian limb as shown in Fig. 15. Since its trajectory was known, MRO tracked TGO producing streaked stars in the background. ONC has also taken inertially-fixed images where moving objects appear streaked relative to a star-field. The ONC capability seems extendable to any sufficiently bright object in Mars orbit.

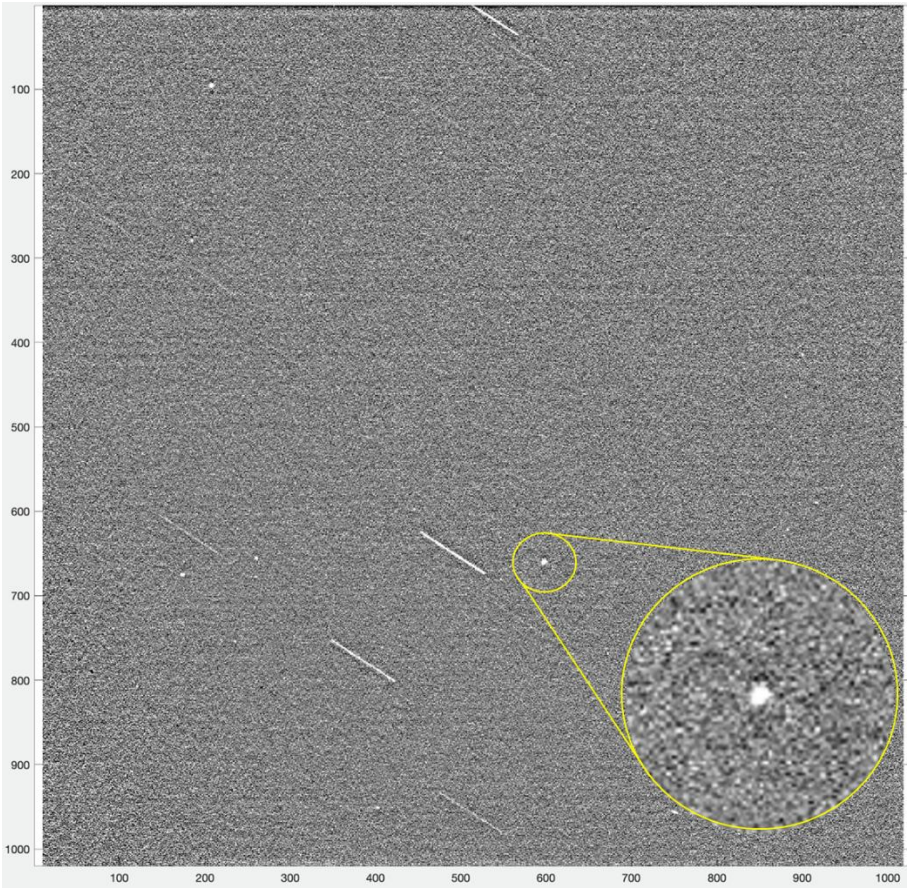

Fig. 15 One in a series of optical detection of the Trace Gas Orbiter (TGO) spacecraft at ~2,700 km range. Several 6th to 9th magnitude stars are streaked in the background. Radiation hits on the CCD are visible as dots.

ONC has an intermittent issue with image quality in a third of the field of view, but otherwise remains functional. Although they are line scanners, CTX and HiRISE are also theoretically capable of detecting in-orbit targets; HiRISE was briefly used to search for the lost Mars Global Surveyor spacecraft [58].

B. DDOR Used to Refine Mars Ephemeris and Mars-bound Spacecraft Trajectories

MRO regularly performs deltaDOR (delta Differenced One-way Ranging) experiments to refine the ephemerides of Mars [56]. This technique uses DSN observations of radio-bright quasars to determine the angular position of a spacecraft relative to those reference quasars as seen by an observer on Earth. The technique is now being extended to use the Mars orbiters themselves as Mars-centric reference points for newly arriving spacecraft. For objects in the vicinity of Mars, this technique eliminates error sources associated with uncertainty in the Mars ephemeris and quasar

positions while also removing errors in tying various coordinate frames together [59]. The MRO and Odyssey spacecraft have now demonstrated this new capability in conjunction with the Europa Clipper spacecraft during its 2025 Mars fly-by. The improved technique was driven by the extreme trajectory accuracy needed for the Mars Sample Return project and presumably would be useful to human missions, as well.

VI. Conclusion

MRO can provide support for future human missions with its array of capabilities. These include finding surface and subsurface water ice, measuring atmospheric density for aerobraking or vehicle control during entry, descent and landing. High and medium resolution imaging and radar measurements of surface roughness support safe landing site selection and extravehicular route planning. Two imagers are capable of documenting hardware location on the surface. At the highest resolution, only ~5% of Mars' surface has been imaged to date. MRO's UHF telecommunication capability could provide not only backup voice communication for astronauts but also service a network for accessing remotely placed equipment. GPS-like position and timing information can be provided by the Electra radio. Both the radio and the imagers function to gather real-time data during EDL for public outreach and for banking that data to enable anomaly investigation in the event of a failure of the incoming vehicle. MRO can track objects in Mars orbit, or on the ground. MRO provides updated ephemeris information for Mars. The use of MRO's accurately known position for determining the trajectory of Mars-bound spacecraft has been demonstrated. MRO functions as a weather satellite and can provide daily updates on clouds and dust storm activity.

We recognize that MRO's collection of capabilities will ultimately be replaced by newer missions. However, some of those missions may not succeed in the first attempt, resulting in a delay in human presence unless existing assets at Mars, such as MRO, remain to fill the role. Once the newer missions are functional, MRO can provide redundancy and/or expanded capability. While MRO has long exceeded its original 5-year design life, there are no known impediments that preclude operation out as far as 2038.

Funding Sources

Work at the Jet Propulsion Laboratory, California Institute of Technology, is performed under contract with the National Aeronautics and Space Administration (80NM0018D0004). The MARCI and CTX work was funded by NASA-NNN12AA01C with subcontract JPL-1515835.

Acknowledgments

ASI provided SHARAD to MRO and leads its operations through a contract to SHARAD Team Leader P. Lombardo at the Sapienza Università di Roma. We thank Sylvain Piqueux, Mark Wronkiewicz and Marek Slipski of JPL for helpful comments on the manuscript.

References

[1] Zurek, R. W., and Smrekar, S. E., "An Overview of the Mars Reconnaissance Orbiter (MRO) Science Mission," *Journal of Geophysical Research*, Vol. 112, 2007. https://doi.org/10.1029/2006JE002701

[2] Johnston, M.D., Graf, J.E., Zurek, R.W., Eisen, H.J. and Jai, B., 2005, March. The Mars reconnaissance orbiter mission. In *2005 IEEE Aerospace Conference* (pp. 447-464). IEEE. https://doi.org/10.1109/aero.2005.1559336

[3] Malin, M. C., Bell, J. F., Cantor, B. A., Caplinger, M., Calvin, W. M., Clancy, R. T., Edgett, K. S., Edwards, L., Haberle, R. M., James, P. B., Lee, S. W., Ravine, M. A., Thomas, P. C., and Wolff, M. J., "Context Camera Investigation on Board the Mars Reconnaissance Orbiter," *Journal of Geophysical Research*, Vol. 112, No. 5, 2007. https://doi.org/10.1029/2006JE002808

[4] Edwards, Charles D. "The Electra Proximity Link Payload for Mars Relay Telecommunications and Navigation." *54th International Astronautical Congress of the International Astronautical Federation, the International Academy of Astronautics, and the International Institute of Space Law*. 2003. https://doi.org/10.2514/6.iac-03-q.3.a.06

[5] McEwen, A. S., Eliason, E. M., Bergstrom, J. W., Bridges, N. T., Hansen, C., Delamere, W. A., Grant, J. A., Gulick, V. C., Herkenhoff, K. E., Keszthelyi, L. P., Kirk, R. L., Mellon, M. T., Squyres, S. W., Thomas, N., and Weitz, C. M., "Mars Reconnaissance Orbiter's High Resolution Imaging Science Experiment (HiRISE)," *Journal of Geophysical Research*, Vol. 112, No. 5, 2007. https://doi.org/10.1029/2005JE002605

[6] Bell III, J.F., Wolff, M.J., Malin, M.C., Calving, W.M., Cantor, B.A., Caplinger, M.A., Clancy, R.T., Edgett, K.S., Edwards, L.J., Fahle, J., Ghaemi, F., Haberle, R.M., Hale, A., James, P.B., Lee, S.W., McConnochie, T., Dobrea, E. Noe, Ravine, M.A., Schaeffer, D., Supulver, K.D., Thomas, P.C., 2009. Mars Reconnaissance Orbiter Mars Color Imager (MARCI): instrument description, calibration, and performance. J. Geophys. Res.-Planets 114, E8. https://doi.org/10.1029/2008JE003315.

[7] McCleese, D. J., Schofield, J. T., Taylor, F. W., Calcutt, S. B., Foote, M. C., Kass, D. M., Leovy, C. B., Paige, D. A., Read, P. L., and Zurek, R. W., "Mars Climate Sounder: An Investigation of Thermal and Water Vapor Structure, Dust and Condensate Distributions in the Atmosphere, and Energy Balance of the Polar Regions," *Journal of Geophysical Research*, Vol. 112, 2007. https://doi.org/10.1029/2006JE002790

[8] Kleinböhl, A., Schofield, J. T., Kass, D. M., Abdou, W. A., Backus, C. R., Sen, B., Shirley, J. H, Lawson, W. G., Richardson, M. I., Taylor, F. W., Teanby, N. A., McCleese, D. J., Mars Climate Sounder Limb Profile Retrieval of atmospheric Temperature, Pressure, Dust and Water ice opacity, J. Geophys. Res., 114, E10006, https://10.1029/2009JE003358, 2009.

[9] Kleinböhl, A., D. M. Kass, M. Schreier, S. Piqueux, S. Suzuki, J. H. Shirley, L. Chen, J. T. Schofield, Far Infrared Radiative Properties of Mars Atmospheric Aerosols and their Application to Mars Climate Sounder Retrievals of Aerosol Profiles, Aerosol Columns and Surface Temperatures, Icarus, 419, 116000, 2024. https://doi.org/10.1016/j.icarus.2024.116000

[10] Stauder, John L., Andrew E. Lowman, Dave Thiessen, Darryl Day, and D. O. Miles. "Off-axis scatter measurement of the Mars reconnaissance orbiter (MRO) optical navigation camera (ONC)." In *Current Developments in Lens Design and Optical Engineering VI*, vol. 5874, pp. 208-219. SPIE, 2005. https://doi.org/10.1117/12.619857

[11] Seu, Roberto, D. Biccari, R. Orosei, L. V. Lorenzoni, R. J. Phillips, Lucia Marinangeli, Giovanni Picardi, A. Masdea, and E. Zampolini. "SHARAD: The MRO 2005 shallow radar." *Planetary and Space Science* 52, no. 1-3 (2004): 157-166. https://doi.org/10.1016/j.pss.2003.08.024

[12] Morgan, G.A., Putzig, N.E., Baker, D.M.H., Pathare, A., Dundas, C.M., Russell, M.B., Perry, M.R., Chojnacki, M., Sizemore, H.G., Bramson, A.M. and Petersen, E.I., 2025. Refined Mapping of Subsurface Water Ice on Mars to Support Future Missions. *The Planetary Science Journal*, *6*(2), p.29. https://doi.org/10.3847/psj/ad9b24

[13] Putzig, Nathaniel E., Gareth A. Morgan, Matthew Perry, Bruce A. Campbell, Jennifer L. Whitten, Fabrizio Bernardini, Alessandro DiCarlofelice, Pier Tognolatti, and Pierfrancesco Lombardo. " HARAD Illuminates Deeper Martian Subsurface Structures with a Boost from Very Large Rolls of the MRO Spacecraft." *The Planetary Science Journal* 6, no. 6 (2025): 140. https://doi.org/10.3847/psj/addbe1

[14] Seelos, F. P., Seelos, K. D., Murchie, S. L., Novak, M. A. M., Hash, C. D., Morgan, M. F., Arvidson, R. E., Aiello, J. J., Bibring, J.-P., Bishop, J. L., Boldt, J. D., Buczkowski, D., Clancy, R. T., Ehlmann, B. L., Frizzell, K. M., Hancock, K. M., Hayes, J. R., Heffernan, K. J., Humm, D. C., Itoh, Y., Ju, M., Kochte, M. C., Malaret, E., McGovern, J. A., McGuire, P., Mehta, N. L., Moreland, E. L., Mustard, J. F., Nair, A. H., Nunez, J. I., O'Sullivan, J. A., Poffenbarger, R. T., Poulet, F., Romeo, G., Santo, A. G., Smith, M. D., Stephens, D., Toigo, A. D., Viviano, C. E., and Wolff, M. J., "The CRISM Investigation in Mars Orbit: Overview, History, and Delivered Data Products," *Icarus*, 2023, p. 115612. https://doi.org/10.1016/j.icarus.2023.115612

[15] McEwen, Alfred S., Shane Byrne, C. Hansen, Ingrid J. Daubar, Sarah Sutton, Colin M. Dundas, Nicole Bardabelias et al. "The high-resolution imaging science experiment (HiRISE) in the MRO extended science phases (2009–2023)." *Icarus* 419 (2024): 115795. https://doi.org/10.1016/j.icarus.2023.115795

[16] Arvidson, R., Adams, D., Bonfiglio, G., Christensen, P., Cull, S., Golombek, M., Guinn, J., Guinness, E., Heet, T., Kirk, R. and Knudson, A., 2008. Mars Exploration Program 2007 Phoenix landing site selection and characteristics. *Journal of Geophysical Research: Planets*, *113*(E3). https://doi.org/10.1029/2007je003021

[17] Golombek, M.P., Huertas, A., Marlow, J., McGrane, B., Klein, C., Martinez, M., Arvidson, R.E., Heet, T., Barry, L., Seelos, K. and Adams, D., 2008. Size-frequency distributions of rocks on the northern plains of Mars with special reference to Phoenix landing surfaces. *Journal of Geophysical Research: Planets*, *113*(E3).https://doi.org/10.1029/2007je003065

[18] Golombek, M., Grant, J., Kipp, D., Vasavada, A., Kirk, R., Fergason, R., Bellutta, P., Calef, F., Larsen, K., Katayama, Y. and Huertas, A., 2012. Selection of the Mars Science Laboratory landing site. *Space science reviews*, *170*, pp.641-737. https://doi.org/10.1007/s11214-012-9916-y

[19] Golombek, M., Kipp, D., Warner, N., Daubar, I.J., Fergason, R., Kirk, R.L., Beyer, R., Huertas, A., Piqueux, S., Putzig, N.E. and Campbell, B.A., 2017. Selection of the InSight landing site. *Space Science Reviews*, *211*, pp.5-95. https://doi.org/10.1007/s11214-016-0321-9

[20] Grant, J. A., Golombek, M. P., Wilson, S. A., Farley, K. A., Williford, K. H., & Chen, A. (2018). The science process for selecting the landing site for the 2020 Mars rover. *Planetary and Space Science*, *164*, 106–126. https://doi.org/10.1016/j.pss.2018.07.001

[21] Fawdon, P., Orgel, C., Adeli, S., Balme, M., Calef, F.J., Davis, J.M., Frigeri, A., Grindrod, P., Hauber, E., Le Deit, L. and Loizeau, D., 2024. The high-resolution map of Oxia Planum, Mars; the landing site of the ExoMars Rosalind Franklin rover mission. *Journal of Maps*, *20*(1), p.2302361. https://doi.org/10.1080/17445647.2024.2302361

[22] Golombek, M.P., Trussell, A., Williams, N., Charalambous, C., Abarca, H., Warner, N.H., Deahn, M., Trautman, M., Crocco, R., Grant, J.A. and Hauber, E., 2021. Rock Size-Frequency Distributions at the InSight Landing Site, Mars. *Earth and Space Science*, *8*(12), p.e2021EA001959. https://doi.org/10.1029/2021ea001959

[23] Sutton, S.S., Chojnacki, M., McEwen, A.S., Kirk, R.L., Dundas, C.M., Schaefer, E.I., Conway, S.J., Diniega, S., Portyankina, G., Landis, M.E. and Baugh, N.F., 2022. Revealing active Mars with HiRISE digital terrain models. *Remote Sensing*, *14*(10), p.2403.https://doi.org/10.3390/rs14102403

[24] Campbell, B.A., Putzig, N.E., Carter, L.M., Morgan, G.A., Phillips, R.J. and Plaut, J.J., 2013. Roughness and near-surface density of Mars from SHARAD radar echoes. *Journal of Geophysical Research: Planets*, *118*(3), pp.436-450. https://doi.org/10.1002/jgre.20050

[25] Putzig, N.E., Morgan, G.A., Campbell, B.A., Grima, C., Smith, I.B., Phillips, R.J. and Golombek, M.P., 2017. Radar-derived properties of the InSight landing site in western Elysium Planitia on Mars. *Space Science Reviews*, *211*, pp.135-146. https://doi.org/ 10.1007/s11214-016-0322-8

[26] Grima, C., Putzig, N.E., Campbell, B.A., Perry, M., Gulick, S.P., Miller, R.C., Russell, A.T., Scanlan, K.M., Steinbrügge, G., Young, D.A. and Kempf, S.D., 2022. Investigating the Martian surface at decametric scale: population, distribution, and dimension of heterogeneity from radar statistics. *The Planetary Science Journal*, *3*(10), p.236. https://doi.org/ 10.3847/PSJ/ac9277

[27] Bussey, B. and Hoffman, S.J., 2016, March. Human Mars landing site and impacts on Mars surface operations. In 2016 IEEE Aerospace Conference (pp. 1-21). IEEE. https://doi.org/10.1109/aero.2016.7500775

[28] Bramson, A.M., Byrne, S., Putzig, N.E., Sutton, S., Plaut, J.J., Brothers, T.C. and Holt, J.W., 2015. Widespread excess ice in arcadia planitia, Mars. Geophysical Research Letters, 42(16), pp.6566-6574. https://doi.org/10.1002/2015gl064844

[29] Morgan, G.A., Putzig, N.E., Perry, M.R., Sizemore, H.G., Bramson, A.M., Petersen, E.I., Bain, Z.M., Baker, D.M., Mastrogiuseppe, M., Hoover, R.H. and Smith, I.B., 2021. Availability of subsurface water-ice resources in the northern mid-latitudes of Mars. Nature Astronomy, 5(3), pp.230-236. https://doi.org/10.1038/s41550-020-01290-z

[30] Putzig, N.E. and Morgan, G.A., Sizemore, H.G., Hollibaugh Baker, D.M., Petersen, E.I., Pathare, A.V., Dundas, C.M., Bramson, A.M., Courville, S.W., Perry, M.R. and Nerozzi, S., 2023. Ice resource mapping on Mars. In Handbook of space resources (pp. 583-616). Cham: Springer International Publishing. https://doi.org/10.1007/978-3-030-97913-3_16

[31] Morgan, G.A. and Putzig, N.E., Baker, D.M.H., Pathare, A., Dundas, C.M., Russell, M.B., Perry, M.R., Chojnacki, M., Sizemore, H.G., Bramson, A.M. and Petersen, E.I., 2025. Refined Mapping of Subsurface Water Ice on Mars to Support Future Missions. *The Planetary Science Journal*, *6*(2), p.29. https://doi.org/10.3847/psj/ad9b24

[32] Amoroso, M., Flamini, E., Ammanito, E., Viotti, M., Mugnuolo, R., Haltigin, T., Boulais, E., Usui, T., Hollibaugh Baker, D.M., Davis, R.M. and Kelley, M.S., 2024, April. International Mars Ice Mapper Mission: Detection, mapping and characterization of subsurface water ice and overburden on Mars with Synthetic Aperture Radar combined with VHF Sounding

and High-Resolution Imaging. In EGU General Assembly Conference Abstracts (p. 10754). https://doi.org/10.5194/egusphere-egu24-10754

[33] Piqueux, S., Buz, J., Edwards, C. S., Bandfield, J. L., Kleinböhl, A., Kass, D. M., Hayne, P. O., The MCS and THEMIS Teams, Widespread shallow water ice on Mars at high latitudes and midlatitudes, Geophys. Res. Lett., 46, 14290–14298, 2019. https://doi.org/10.1029/2019gl083947

[34] Cushing, G.E., Okubo, C.H. and Titus, T.N., 2015. Atypical pit craters on Mars: New insights from THEMIS, CTX, and HiRISE observations. *Journal of Geophysical Research: Planets*, *120*(6), pp.1023-1043. https://doi.org/10.1002/2014je004735

[35] Gladden, R., Anabtawi, A., Buccino, D., Call, J., Chamberlain, N., Elliott, H., ... & Srnka, E. (2022, March). Preparing the Mars relay network for the arrival of the perseverance rover at Mars. In *2022 IEEE Aerospace Conference (AERO)* (pp. 01-19). IEEE. https://doi.org/10.1109/aero53065.2022.9843762

[36] Tamppari, L.K., Barnes, J., Bonfiglio, E., Cantor, B., Friedson, A.J., Ghosh, A., Grover, M.R., Kass, D., Martin, T.Z., Mellon, M. and Michaels, T., 2008. Expected atmospheric environment for the Phoenix landing season and location. *Journal of Geophysical Research: Planets*, *113*(E3). https://doi.org/10.1029/2007je003034

[37] Blanchard, R. C., P. N. Desai, Mars Phoenix Entry, Descent, and Landing Trajectory and Atmosphere Reconstruction, J. Spacecraft Rockets 48, 809-821, 2011. https://doi.org/10.2514/1.46274

[38] Vasavada, A.R., Chen, A., Barnes, J.R., Burkhart, P.D., Cantor, B.A., Dwyer-Cianciolo, A.M., Fergason, R.L., Hinson, D.P., Justh, H.L., Kass, D.M. and Lewis, S.R., 2012. Assessment of environments for Mars Science Laboratory entry, descent, and surface operations. *Space Science Reviews*, *170*, pp.793-835. https://doi.org/10.1007/978-1-4614-6339-9_21

[39] Chen, A., A. Cianciolo, A. R. Vasavada, C. Karlgaard, J. Barnes, B. Cantor, D. Kass, S. Rafkin, D. Tyler, Reconstruction of Atmospheric Properties from Mars Science Laboratory Entry, Descent, and Landing, J. Spacecraft Rockets 51, 1062-1075, 2014. https://doi.org/10.2514/1.a32708

[40] Golombek, M., Kass, D., Williams, N., Warner, N., Daubar, I., Piqueux, S., Charalambous, C. and Pike, W.T., 2020. Assessment of InSight landing site predictions. *Journal of Geophysical Research: Planets*, *125*(8), p.e2020JE006502. https://doi.org/10.1029/2020je006502

[41] Karlgaard, C. D., E. P. Bonfiglio, D. M. Kass, M. R. Grover, Mars InSight Entry, Descent, and Landing Trajectory and Atmosphere Reconstruction, J. Spacecraft Rockets 58, 865-878, 2021. https://doi.org/10.2514/6.2020-1271

[42] Mischna, M. A., G. Villar, D. M. Kass, S. Dutta, S. Rafkin, D. Tyler, J. Barnes, B. Cantor, S. R. Lewis, D. Hinson, J. Pla-García, A. Kleinböhl, C. Karlgaard, Pre- and Post-entry, Descent and Landing Assessment of the Martian Atmosphere for the Mars 2020 Rover, Planet. Sci. J. 3, 147, 2022. https://doi.org/10.3847/psj/ac7148

[43] Malin, M.C., Calvin, W.M., Cantor, B.A., Clancy, R.T., Haberle, R.M., James, P.B., Thomas, P.C., Wolff, M.J., Bell III, J.F., Lee, S.W., 2008. Climate, weather, and north polar observations from the Mars Reconnaissance Orbiter Mars Color Imager. Icarus 194, 501–512. https://doi.org/10.1016/j.icarus.2007.10.016.

[44] Cantor, B.A., James, P.B., Calvin, W.M., 2010. MARCI and MOC observations of the atmosphere and surface cap in the north polar region of Mars. Icarus 208 (1), 61–81, https://doi.org/10.1016/j.icarus.2010.01.032.

[45] Calvin, W. M., James, P. B., Cantor, B. A., and Dixon, E. M., 2015. Interannual and seasonal changes in the north polar ice deposits of Mars: Observations from MY 29–31 using MARCI. Icarus 251, 181-190. http://dx.doi.org/10.1016/j.icarus.2014.08.026.

[46] Clancy, R.T., Wolff, M.J., Lefevre, F., Cantor, B.A., Malin, M.C., Smith, M.D., 2016. Daily global mapping of Mars ozone column abundances with MARCI UV band imaging. Icarus 266, 112–133. https://doi.org/10.1016/j.icarus.2015.11.016.

[47] Wolff, M. J., Clancy, R. T., Kahre, M. A., Haberle, R. M., Forget, F., Cantor, B. A., and Malin, M. C., 2019. Mapping water ice clouds on Mars with MRO/MARCI. Icarus 332, 24–49. https://doi.org/10.1016/j.icarus.2019.05.041

[48] Clancy, R.T., Wolff, M.J., Smith, M.D., Kleinb¨ ohl, A., Cantor, B.A., Murchie, S.L., Toigo, A.D., Seelos, K., Lefevre, F., Montmessin, F., Daerden, F., Sandor, B.J., 2019. The distribution, composition, and particle properties of Mars mesospheric

aerosols: an analysis of CRISM visible/near-IR limb spectra with context from near-coincident MCS and MARCI observations. Icarus 328, 246–273. https://doi.org/10.1016/j.icarus.2019.03.025.

[49] Clancy, R.T., Wolff, M.J., Heavens, N.G., James, P.B., Lee, S.W., Sandor, B.J., Cantor, B. A., Malin, M.C., Tyler Jr., D., Spiga, A., 2021. Mars perihelion cloud trails as revealed by MARCI: Mesoscale topographically focused updrafts and gravity wave forcing of high-altitude clouds. Icarus 362. https://doi.org/10.1016/j.icarus.2021.114411.

[50] Cantor, B., Pickett, N., Malin, M.C., Lee, S.W., Wolff, M.J., Caplinger, M.A., 2019. Martian dust storm activity near the Mars 2020 candidate landing sites: MRO-MARCI observations from Mars years 28-34. Icarus 321 (15), 161–170. https://doi.org/10.1016/j.icarus.2018.10.005.

[51] Bridges, J.C., Clemmet, J., Croon, M., Sims, M.R., Pullan, D., Muller, J.P., Tao, Y., Xiong, S., Putri, A.R., Parker, T. and Turner, S.M.R., 2017. Identification of the Beagle 2 lander on Mars. *Royal Society Open Science*, *4*(10), p.170785. https://doi.org/10.1098/rsos.170785

[52] CCSDS INFORMATIONAL REPORT on Voice Communications, Green Book, CCSDS 706.2-G-2, December 2018. https://ccsds.org/Pubs/706x2g2.pdf

[53] Edwards, C.D., Bell, D.J., Gladden, R.E., Ilott, P.A., Jedrey, T.C., Johnston, M.D., Maxwell, J.L., Mendoza, R., McSmith, G.W., Potts, C.L. and Schratz, B.C., 2013, March. Relay support for the mars science laboratory mission. In *2013 IEEE Aerospace Conference* (pp. 1-14). IEEE. https://doi.org/10.1109/aero.2013.6497325

[54] Arvidson, R.E., Ashley, J.W., Bell III, J.F., Chojnacki, M., Cohen, J., Economou, T.E., Farrand, W.H., Fergason, R., Fleischer, I., Geissler, P. and Gellert, R., 2011. Opportunity Mars Rover mission: Overview and selected results from Purgatory ripple to traverses to Endeavour crater. *Journal of Geophysical Research: Planets*, *116*(E7). https://doi.org/10.1029/2010je003746

[55] Guinn, Joseph R., Joseph E. Riedel, Shyam Bhaskaran, Ryan S. Park, Andrew T. Vaughan, William M. Owen, Todd Ely, Matthew Abrahamsson, and Tomas Martin-Mur. "The deep-space positioning system concept: Automating complex navigation operations beyond the earth." In *AIAA SPACE 2016*, p. 5409. 2016. https://doi.org/10.2514/6.2016-5409

[56] Perino, Scott, Darren Cooper, David Rosing, Louis Giersch, Zach Ousnamer, Vahraz Jamnejad, Carl Spurgers et al. "The evolution of an orbiting sample container for potential Mars sample return." In *2017 IEEE Aerospace Conference*, pp. 1-16. IEEE, 2017. https://doi.org/10.1109/aero.2017.7943979

[57] Mattingly, Richard, Steve Matousek, and Frank Jordan. "Continuing evolution of Mars sample return." *2004 IEEE Aerospace Conference Proceedings (IEEE Cat. No. 04TH8720)*. Vol. 1. IEEE, 2004. https://doi.org/10.1109/aero.2004.1367630

[58] McEwen, A.S., Banks, M.E., Baugh, N., Becker, K., Boyd, A., Bergstrom, J.W., Beyer, R.A., Bortolini, E., Bridges, N.T., Byrne, S. and Castalia, B., 2010. The high resolution imaging science experiment (HiRISE) during MRO's primary science phase (PSP). *Icarus*, *205*(1), pp.2-37. https://doi.org/10.1016/j.icarus.2009.04.023

[59] Melbourne, W. and Curkendall, D., 1977. Radio metric direction finding: a new approach to deep space navigation. In *Astrodynamics Conference* (p. 3188). https://doi.org/10.2514/6.1978-3188